Atmos. Chem. Phys. Discuss., 11, 28169–28217, 2011
www.atmos-chem-phys-discuss.net/11/28169/2011/
doi:10.5194/acpd-11-28169-2011

Atmospheric Chemistry and Physics Discussions

Error characterization of CO_2 vertical mixing in the atmospheric transport model WRF-VPRM

R. Kretschmer, C. Gerbig, U. Karstens, and F.-T. Koch

Max Planck Institute for Biogeochemistry, Jena, Germany

Received: 28 August 2011 – Accepted: 27 September 2011 – Published: 20 October 2011

Correspondence to: R. Kretschmer (rkretsch@bgc-jena.mpg.de)

Published by Copernicus Publications on behalf of the European Geosciences Union.

Abstract

One of the dominant uncertainties in inverse estimates of regional CO_2 surface-atmosphere fluxes is related to model errors in vertical transport within the planetary boundary layer (PBL). In this study we present the results from a synthetic experiment using the atmospheric model WRF-VPRM to realistically simulate transport of CO_2 for large parts of the European continent at 10 km spatial resolution. To elucidate the impact of vertical mixing error on modeled CO_2 mixing ratios we simulated a month during the growing season (August 2006) with different commonly used parameterizations of the PBL (Mellor-Yamada-Janjic (MYJ) and Yonsei-University (YSU) scheme). To isolate the effect of transport errors we prescribed the same CO_2 surface fluxes for both simulations. Differences in simulated CO_2 mixing ratios (model bias) were on the order of 3 ppm during daytime with larger values during night. We present a simple method to reduce this bias by 70–80 % when the true height of the mixed layer is known.

1 Introduction

Anthropogenic emissions of greenhouse gases (GHG) have changed the atmospheric composition substantially (IPCC, 2007). Carbon dioxide (CO_2) and methane (CH_4) were identified as the most important GHG for the anthropogenic alterations of the global climate system. The carbon cycle is linked to climate directly by affecting the energy budget of the Earth and indirectly via feedback processes (Heimann and Reichstein, 2008). Oceans and terrestrial biosphere are slowing down this process by absorbing about half of the anthropogenic carbon emissions (Canadell et al., 2007). The spatial distribution, strength and temporal development of these sinks is subject to active research. However, multilateral treaties like the Kyoto protocol aim at the reduction and management of the anthropogenic emissions in order to mitigate the human impact on the climate system. Thus, improved knowledge on carbon budgets is the basis to project future climate, to support political discourse, to verify emission inventories and to monitor management techniques of the carbon cycle.

ACPD
11, 28169–28217, 2011

In the past inversions of global CO_2 measurements were used in an "top-down" approach (Nisbet and Weiss, 2010) to infer carbon fluxes for regions the size of continents (e.g. Schimel et al., 2001; Gurney et al., 2002) down to spatial scales of 100 km (Rödenbeck et al., 2003; Peters et al., 2007). To relate carbon source/sink processes to external forcing on the sub-continental scale, where the observed CO_2 signals near vegetated areas are highly variable and flux signatures degrade rapidly due to mixing in the lower troposphere, inversion frameworks with even higher spatio-temporal resolutions (<100 km, diurnal) are a necessity (Gerbig et al., 2003; Karstens et al., 2006; Gerbig et al., 2009; Lauvaux et al., 2009; Göckede et al., 2010).

In inversions the causal link between CO_2 mixing ratios and sources/sinks is represented by atmospheric transport models. It is known for quite some time that these models are subject to uncertainties that hamper reliable estimations of surface fluxes significantly (Law et al., 1996; Gerbig et al., 2003; Stephens et al., 2007; Law et al., 2008; Lauvaux et al., 2009; Houweling et al., 2010). Especially at high spatio-temporal resolution different sources of transport error were reported. Lin and Gerbig (2005) amount the impact of misrepresenting wind flows in the transport model on CO_2 concentration during the active growing season to ~6 ppm. Inaccurate representation of meteorological processes at the meso- and microscale, e.g. land-see breezes, mountain-valley circulations, heat island effects and surface energy fluxes can cause errors of ~2–3 ppm (Ahmadov et al., 2007; van der Molen and Dolman, 2007; Tolk et al., 2008).

One of the dominant transport uncertainties is related to vertical mixing of CO_2 associated with atmospheric turbulence near the surface where most CO_2 observations are made. Errors in vertical transport, that exceed the targeted measurement precision for CO_2 of 0.1 ppm by more than an order of magnitude, are inflicted by the seasonal and diurnal covariances of CO_2 fluxes and turbulence in the planetary boundary layer (PBL) (Denning et al., 1995, 1996, 1999, 2008; Stephens et al., 2000; Yi et al., 2001b, 2004; Gerbig et al., 2008; Tolk et al., 2009).

ACPD
11, 28169–28217, 2011

On the diurnal scale, several vertical mixing processes affect the course of CO_2 in the PBL. During daytime, photosynthetic uptake is diluted up to the height of a turbulent mixed layer (ML) within the convective boundary layer (CBL) on hourly time scales. Thermals may overshoot the ML and cause entrainment of free tropospheric air. On average such processes can affect time-mean CO_2 concentrations in the mixed layer on the order of several ppm, but also alter other properties of the ML like moisture, temperature and the mixing height itself (McGrath-Spangler and Denning, 2010).

Due to the vigorous mixing in the CBL on small timescales variables like potential temperature, water vapor and CO_2 approximate constant vertical profiles (Stull, 1988). In fact, various studies used this simplification for column mass budgeting approaches to directly determine CO_2 exchange fluxes (e.g. Wofsy et al., 1988; Chou et al., 2002; Laubach and Fritsch, 2002; Bakwin et al., 2004; Helliker et al., 2004; Aubinet et al., 2005b).

When turbulence ceases as less radiation heats the surface after sunset the colder air layer near the surface is decoupled from the warmer well mixed part of the ML. During these times the latter, termed residual layer (RL), is not directly affected by surface forcings, because air parcels are confined to the lower part of the PBL by the capping temperature inversion. Hence, tracer profiles in the RL stay relatively constant with time (Yi et al., 2001b). In the night, respiration fluxes dominate and cause accumulation of CO_2 in a shallow stable boundary layer (SBL) below the RL. In the SBL mixing can occur due to wind shear and surface friction up to several 100 m (Stull, 1988). In other situations mixing may be too weak and trace gases like CO_2 accumulate near the surface. When sun rises again the capping inversion is getting weaker due to increased heat fluxes into the SBL. During the growth of the new mixed layer RL air is entrained, which causes a rapid dilution of CO_2 molecules (Gibert et al., 2007).

The mixing height (MH, z_i), normally a property of the CBL, is an intuitive measure for vertical mixing strength because it is defined as the level of most negative heat flux or also as the height at which air parcels rising from the surface become

ACPD
11, 28169–28217, 2011

neutrally buoyant (Stull, 1988). The MH not only determines the volume of a column of air in which the fluxes contribute to the CO_2 concentration, model mismatches in this property can also lead to bias in CO_2 (Denning et al., 1996, 2008; Yi et al., 2004; Pérez-Landa et al., 2007; Ahmadov et al., 2009). Ramonet et al. (2009) and Aulagnier et al. (2010) demonstrated that variations of the MH is an important driver for a recently observed build up of CO_2 over the European continent. In an intercomparison study of 5 mesoscale tracer models Sarrat et al. (2007) conclude that MHs between models revealed considerable discrepancies. Gerbig et al. (2008) (hereafter G08) demonstrated that MH uncertainties relate to CO_2 transport errors of 3 ppm during summertime.

In this paper we further investigate the relationship between mixing height and CO_2 concentrations in the PBL. Similar to G08 we assume that errors in simulated PBL CO_2 concentrations are to a first order caused by a wrong vertical distribution of CO_2 in a given atmospheric column, such that the column integrated concentration is unaffected. Thus, one might correct for the error in simulated PBL CO_2 by redistributing or reshuffling CO_2 from the free troposphere to the PBL or vice versa, compensating for the mismatch between true and observed mixing height, while keeping the total column mass unchanged. We present the results of a pseudo-data experiment using the high resolution chemical transport model WRF-VPRM (Ahmadov et al., 2007). It was set up with two parameterizations of the PBL: the Mellor-Yamada-Janjić (MYJ, Janjic, 2002) and the Yonsei-University (YSU, Hong et al., 2006) scheme. Hereafter we refer to the simulations with the different schemes as MYJ and YSU respectively. Both schemes are commonly used parameterizations which are able to realistically simulate PBL dynamics (e.g. Borge et al., 2008). In addition, we diagnose biospheric fluxes from satellite reflectance data at 500 m horizontal resolution updated every 8 days and use the recent 2005 EDGAR emission inventory to consider anthopogenic flux contributions. In line with previous findings (Ahmadov et al., 2007; Sarrat et al., 2007; Ahmadov et al., 2009; Pillai et al., 2010) we therefore assume the simulated CO_2 fields to realistically capture the dominant mixing and flux processes that determine the diurnal variation of atmospheric CO_2 concentration. However, it is also known that MYJ produces weaker

ACPD
11, 28169–28217, 2011

vertical mixing compared to YSU and other schemes (Hu et al., 2010), thus these two schemes seem appropriate for the purpose of our study as significant divergence in simulated transport of CO_2 can be expected as well.

The goal of our study is to investigate the following scientific questions:

1. How large are the discrepancies in simulated mixed layer heights?
2. What is the quantitative impact of theses differences on the simulated CO_2 (i.e. transport model error)?
3. Can we use the true mixing height to reduce this model error?

We diagnose and compare the simulated mixing height to determine errors in vertical mixing. The simulation using the YSU scheme is defined as known truth, and the MYJ simulation as potentially error prone model. Regarding the third question this paper can be seen as a preparatory study to elucidate the potential for assimilating observation based mixing heights into the modeling system to better constrain vertical transport.

We organized the paper as follows. In the method section we describe the WRF-VPRM modeling system and present the reshuffling method used to vertically redistribute CO_2. To test this method we apply it to a 1-D conceptual model of the PBL and to the WRF-VPRM simulated 3-D CO_2 fields. In the result section we show the comparison of the WRF-VPRM simulations in terms of mixing heights and CO_2 concentration together with the results of the pseudo-data experiment. The discussion focuses on shortcomings of our method as well application to current regional inversions.

2 Methodology

2.1 WRF-VPRM modeling system and its setup

We applied the WRF-VPRM modeling system (Ahmadov et al., 2007) to simulate biospheric fluxes and transport of CO_2 for large parts of the European continent during

ACPD
11, 28169–28217, 2011

the period August 2006 in forecast mode (30 h short range forecasts). The chosen horizontal resolution is 10 km at 41 vertical levels with the model top at 50 hPa. The lowest vertical level has a thickness of ~35 m and 19 levels are below 2 km height above ground. The model domain is shown in Fig. 1. Each of the 30 h short-term forecasts comprise 6 h of meteorology spin-up. We excluded water grid cells from the analysis of the simulation output since the focus of our study is on PBL simulation over land. In addition, 10 grid cells at each domain border were excluded to minimize direct influence of the lateral boundary conditions. An overview over the used physic options is given in Table 1.

What follows is a brief review of the main model components, for a more detailed model description the reader is referred to Ahmadov et al. (2007).

WRF-VRPM couples the Weather Research and Forecasting model (http://www.wrf-model.org) to the Vegetation Photosynthesis and Respiration Model (VPRM, Mahadevan et al., 2008). WRF is a mesoscale non-hydrostatic numerical weather prediction model which was extended by Grell et al. (2005) to allow for atmospheric transport of chemical compounds and aerosols on-line (WRF-Chem). Ahmadov et al. (2007) added transport of CO_2 as passive tracer to WRF-Chem in such a way that separation of the different CO_2 components (background, anthropogenic, biospheric) is possible.

VPRM calculates hourly biosphere-atmosphere CO_2 exchange fluxes diagnostically as a function of WRF surface temperature (T2), short wave radiation (SWDOWN) fields and two indices: the Enhanced Vegetation Index (EVI) and the Land Surface Water Index (LSWI) derived from MODIS (Moderate Resolution Imaging Spectroradiometer) satellite surface reflectance retrievals given globally at 500 m horizontal resolution at 8 day intervals. The VPRM calculations are scaled by parameters specific to the vegetation coverage of the model grid cell. These parameters were optimized against eddy covariance flux measurements for the North American continent (Mahadevan et al., 2008). Here we use updated parameters suitable for the European continent (Pillai et al., 2011). The fractional vegetation coverage for the model grid is obtained from the SYNMAP (Jung et al., 2006) with a spatial resolution of 1 km.

ACPD
11, 28169–28217, 2011

To isolate the effect of vertical mixing mismatches on the CO_2 concentrations we prescribed the same VPRM fluxes for both simulations. Technically, VPRM fluxes were first calculated within the YSU simulation and then added to the MYJ simulation as flux input field similar to the anthropogenic emissions.

Hourly CO_2 fluxes from anthropogenic sources were prescribed with 2005 data obtained from the Emissions Database for Global Atmospheric Research (EDGAR) version 4.1 (0.1×0.1 degree grid, http://edgar.jrc.ec.europa.eu). Oceanic flux contributions are considered solely as part of the initial and later boundary conditions from the global model (see paragraph below), i.e. they are not explicitly prescribed in the short-term forecasts, because compared to the biospheric fluxes, oceanic fluxes are small and vary only slightly and because our analysis excludes ocean grid cells entirely.

Lateral boundary conditions of the meteorology, sea surface temperature and soil initialization fields were taken from ECMWF analysis (European Center for Medium-Range Weather Forecasts, 6 hourly, 35 km horizontal resolution). CO_2 initial and boundary conditions were obtained from TM3 inversion results driven by NCEP meteorology (Rödenbeck, 2005)[1]. To account for CO_2 flushing time of the domain we excluded the first 8 days from the simulated period (2–30 August 2006) from our analysis.

We refer the reader to previous studies which have shown the capability of WRF-VPRM to realistically simulate atmospheric transport of CO_2, e.g. Ahmadov et al. (2007), Sarrat et al. (2007), Ahmadov et al. (2009), Pillai et al. (2010), Pillai et al. (2011).

2.2 Reshuffling method for mixed layer CO_2

In this section we describe a method to relate model-model (or model-truth) differences of mixed layer CO_2 and mixing height. Figure 2 illustrates two simplified profiles of CO_2 in the atmosphere. This concept is based on simple slab model considerations

[1] http://www.bgc-jena.mpg.de/~christian.roedenbeck/download-CO2/

ACPD
11, 28169–28217, 2011

assuming convective conditions in the afternoon and an infinitesimally thin entrainment zone (Stull, 1988).

We define one profile as the true (mixing height $z_{i,\mathrm{truth}}$) and the other one as modeled column ($z_{i,\mathrm{model}}$). Assuming the same total mass and CO_2 fluxes for both columns (photosynthetic uptake during day), the mean mole fraction in the model ML ($C_{\mathrm{m,model}}$) is lower than the true mean mixing ratio ($C_{\mathrm{m,truth}}$). This is because in the model photosynthesis removes CO_2 molecules at the same rate from a shallower volume (surface to $z_{i,\mathrm{model}}$ and unit area). Knowing the true mixing height one can adjust $C_{\mathrm{m,model}}$ to match the true mixing ratio by reshuffling air between the mixed layer and the air just above the ML (with mixing ratio C_+), while keeping the total column integrated mass of CO_2 fixed (G08). Mathematically this is expressed as follows:

$$C_{\mathrm{m,truth}} = (C_{\mathrm{m,model}} - C_+) \frac{\int_0^{z_{i,\mathrm{model}}} \rho(z)\, dz}{\int_0^{z_{i,\mathrm{truth}}} \rho(z)\, dz} + C_+ \quad (1)$$

with

$$C_{\mathrm{m,truth}} = \frac{1}{z_{i,\mathrm{truth}}} \int_0^{z_{i,\mathrm{truth}}} C(z)\, dz$$

and

$$C_{\mathrm{m,model}} = \frac{1}{z_{i,\mathrm{model}}} \int_0^{z_{i,\mathrm{model}}} C(z)\, dz$$

where $\rho(z)$ and $C(z)$ are profiles of molar air density and mole fraction mixing ratio of CO_2 respectively. Effectively this method entrains the air between $z_{i,\mathrm{model}}$ and $z_{i,\mathrm{truth}}$ into the ML which gets perfectly mixed instantaneously to yield $C_{\mathrm{m,truth}}$. Similarly, when the model overestimates the mixing height, the method "unmixes" by turning the air between $z_{i,\mathrm{truth}}$ and $z_{i,\mathrm{model}}$ into free tropospheric or residual layer air, depending on the layer above the mixing height. During nighttime when respirative fluxes dominate (net gain of CO_2 molecules) the relationship between MH and mixing ratio reverses.

ACPD
11, 28169–28217, 2011

A special case of the column approach is to assume a height constant air density profile. Such approximation is usually made when the profiles of density and CO_2 are not known (Laubach and Fritsch, 2002). Under these considerations Eq. (1) can be simplified to

$$C_{\mathrm{m,truth}} = (C_{\mathrm{m,model}} - C_+) \frac{z_{i,\mathrm{model}}}{z_{i,\mathrm{truth}}} + C_+ \quad (2)$$

We use this simplification because for the scaling only the MHs have to be known. For the WRF simulated meteorology the absolute differences between the ratio of densities in Eq. (1) and the MH ratios were on average in the range of 9–17 % with standard deviations of 7–9 %. Lower values were calculated during nighttime.

The presented correction method Eq. (2) will be tested in the following section with a conceptual 1-D model of the PBL.

2.3 Test of the reshuffling method

The reshuffling method (Eq. 2) was tested with a conceptual model of the PBL. We base our concept model on a simplified mass budget equation as used in the past to constrain CO_2 fluxes and isotopes of CO_2 from observed concentrations and meteorological properties (e.g. Laubach and Fritsch, 2002; Helliker et al., 2004; Aubinet et al., 2005a). Although this model is subject to several simplifying assumption (in detail discussed in the literature mentioned) it can realistically describe the diurnal evolution of CO_2 concentration in the PBL.

Here we use a height integration formulation which was applied to analyze data from the Amazon Boundary Layer Experiment (ABLE) (Stephens et al., 2000; Chou et al., 2002; Wofsy et al., 1988):

$$\rho \frac{\partial (z_i\, C_{\mathrm{m}})}{\partial t} = F_{\mathrm{NEE}} + \rho \left(\bar{w}_{z_i} - \frac{\partial z_i}{\partial t}\right) (C_{\mathrm{m}} - C_+) \quad (3)$$

The mean mixing ratio (C_{m}) of CO_2 in the mixed layer with height (z_i) is balanced by the surface biospheric fluxes F_{NEE}, entrainment and vertical advection (second term on

ACPD
11, 28169–28217, 2011

the RHS). For simplicity we keep the dry air molar density ρ vertically and temporally constant, and contributions to the mass balance from horizontal advection is neglected. The subsidence is included in the last term on the RHS, it accounts for vertical advection at the top of the ML (with mean velocity $\bar{w}_{z_i}$) that mixes concentrations directly above the ML (C_+) and the ML concentration (C_m).

A simple model based on Eq. (3) was time integrated for several days to compute the variation of the CO_2 within a column of air with unit area and a fixed height of $h = 3.3$ km. The whole column is advected downwards with a temporally fixed subsidence rate which is set to typical values for the mid-latitudes (Stull, 1988; Yi et al., 2001a). At the column top (h) this is set to $\bar{w}_h = -0.02\,\mathrm{m\,s^{-1}}$ and linearly drops to $\bar{w}_0 = 0\,\mathrm{m}\,s^{-1}$ at the surface, representing constant horizontal divergence. This profile is used to obtain subsidence velocity at the MH ($\bar{w}_{z_i}$). We prescribe the flux of CO_2 (F_{NEE}) with typical values for mid-latitudes continental vegetation (Dolman et al., 2006; Ahmadov et al., 2007; Gibert et al., 2007) as a net sink over 24 h ($\sim -3.4\,\mu\mathrm{mol\,s^{-1}}$, Fig. 3a). The background CO_2 mixing ratio is set to the constant value of 380 ppm (C_t). Growth and decay of the mixed layer over 24 h are prescribed as shown in Fig. 3a.

In order to test the reshuffling method (Eq. 2), a second run with a 30 % low bias in mixing heights was performed (blue line in Fig. 3a). We will refer to this run in this section as the model, while the original run (red line in Fig. 3a) represents the truth with stronger vertical mixing (referred to in this section as truth).

Both runs start with a constant CO_2 profile of 380 ppm at each model layer (264 layers each 12.5 m thick). After 14 days of integration (time steps of 150 s) the model reaches steady state, i.e. fluxes and storage of ML CO_2 in Eq. (3) are balanced.

The resulting model mismatch of mixed layer CO_2, i.e. the differences between truth and model ($C_{m,model} - C_{m,truth}$), is shown in Fig. 3b (black line). According to the prescribed CO_2 fluxes the difference is positive during nighttime and negative during daytime. In the following we will refer to these differences generally as CO_2 mismatch.

Applying the reshuffling method (Eq. 2) based on the true MH ($z_{i,truth}$) to correct the model ML CO_2 mixing ratio ($C_{m,model}$, Fig. 3b red line), the CO_2 mismatch is completely

ACPD
11, 28169–28217, 2011

removed during daytime (10:00 to 14:00 local time). In the later afternoon, during nighttime, and in the early morning the correction can reduce the difference, but exhibits overcompensation. The reason is the compensating effect of night and daytime differences due to sign reversal.

The simulated profiles in Fig. 4 show that during these times an residual layer (RL) is situated above the ML, which determines the mean CO_2 mixing ratio above the ML C_+ in Eq. (2). The RL concentration is lower in the model according to equally lower ML values during daytime. As such it preserves the daytime CO_2 mismatch over time. Thus, the temporally local reshuffling is obviously insufficient in these cases. Consequently the information the RL mixing ratios contain can be used to extend the reshuffling method. An improved correction method addresses the biased RL concentration before correcting the ML concentration. This correction can be accomplished with the same reshuffling method applied first to the RL (reshuffle air between free troposphere and RL) and afterwards using the corrected RL mixing ratio in Eq. (2) to also adjust the ML, given the true and modeled height of the RL is known. Figure 3b (blue line) shows the result of applying such a second order correction which removes the CO_2 mismatch for the full period. Thus we conclude that the reshuffling method can fully compensate the CO_2 mismatch in a 1-D model. We hypothesize that errors made due to the simplifications of the 1-D model are small compared to the mixing height induced CO_2 mismatches. In the remainder of the paper we will test this hypothesis in the complex 3-D WRF simulation. As a prerequisite it is necessary to diagnose the mixing heights from the simulated meteorology. This is discussed in the following section.

2.4 Estimation of mixing height

Estimating the simulated mixing height is a non-trivial task. Both PBL schemes diagnose the PBL height online from the model state differently (see Appendix A for details). This height is not necessarily equivalent to the MH, i.e. the level up to which the CO_2 profile is nearly constant with height. In our PBL concept the transition zone from the well mixed part to the free troposphere (entrainment zone) is assumed to be infinitesimally thin. This is different for the complex 3-D simulation and thus it matters where

ACPD
11, 28169–28217, 2011

exactly the diagnosed PBL top is located. For instance the ML mean CO_2 mixing ratio is different if the PBL scheme places the mixing height in or above the entrainment zone or to somewhere much closer to the ML. Because the MH would ideally be located at the top of the well mixed part of the PBL, the mean mixing ratio of CO_2 (C_m) integrated up to this height z_i will be different from the mean mixing ratio arising from a given diagnosed PBL height z_{PBL} (schematically shown in Fig. 5). We can regard this difference of mixing ratios as an error ΔC_m of the calculated mean mole fraction C_m:

$$\Delta C_m = \frac{1}{z_{PBL}} \int_0^{z_{PBL}} C(z)\, dz - \frac{1}{z_i} \int_0^{z_i} C(z) dz \quad (4)$$

Since both PBL schemes use their own diagnosing method for the PBL top this error ΔC_m may even be inconsistent between both schemes, which would affect the results of our study. One option might be to consider the CO_2 gradient between ML and free troposphere to determine the MH, but in reality this information is usually not available since CO_2 profiles are measured only sparsely or in such a way that the measured profile covers only the lowest 100 m. Accordingly, we decided to restrict ourselves to a method that more generally diagnoses the PBL top rather than mixing height itself, knowing that this approach will cause some error of the PBL CO_2 averages ($\Delta C_m \neq 0$ ppm).

If ΔC_m is consistently arising for both simulations, the CO_2 mismatch will be similar Therefore, we tested independent methods to derive the MH offline from the simulated meteorology. Similar to G08 we applied the Bulk-Richardson number method (Eq. 1 in Vogelezang and Holtslag (1996), hereafter VH96) with the critical Richardson number $Ri_c = 0.25$. Offline and online derived MHs differed only slightly in the YSU simulation, which is not surprising since the YSU scheme also bases its diagnostic on a Bulk-Richardson calculation (Appendix A). In contrast the offline diagnosed heights for the MYJ simulation were in general much higher than online calculated ones. We tested two other versions of the Bulk-Richardson number method (Eqs. 2 and 3 of VH96). We got nearly similar results, but for the nighttime the height differences between MYJ and YSU even changed sign when using different methods.

ACPD
11, 28169–28217, 2011

To see which of these different diagnosed heights are most consistent with the actually simulated CO_2 profile we compared ΔC_m. For the calculation of the second term on the RHS of Eq. (4) we used half the diagnosed PBL top z_{PBL} for z_i in cases with a well developed ML. This seems to be a reasonable choice because the entrainment zone can be $0.4\,z_i$ thick (Stull, 1988) and in well mixed conditions the mean mole fraction C_m is equal $C(z)$ for any height z below the ML top. We used the criterion $z_{PBL} > 600$ m for the choice of well developed ML cases.

As example we show the results for the monthly averaged ΔC_m at 12:00 UTC in Fig. 6. As expected the averages for ΔC_m are nearly identical when integrated over offline and online diagnosed PBL height in the YSU case. Both times the PBL top and as a consequence also the PBL CO_2 averages (C_{PBL}) are much higher than the CO_2 within the ML, because too much CO_2 enriched air from the free troposphere was integrated. For MYJ one can clearly see that the online diagnosed PBL top is more appropriate and that ΔC_m is of the same size as for the YSU case.

A possible explanation for this result might be a combination of how the threshold of the TKE (turbulent kinetic energy) that defines the PBL top in the MYJ scheme was chosen and how the transport of scalars in the PBL is related to this height (Appendix A). Similar results were reported by Hu et al. (2010) who applied the 1.5-theta-increase method to calculate the MYJ PBL height offline.

Because of this result we decided to proceed using the WRF diagnosed PBL heights for our study since it seems to relate better to the effective MH for both schemes and ΔC_m is consistent between the two schemes. For simplicity we will not longer distinguish between PBL top and mixed layer height in the remainder of this paper and will refer to the diagnosed height just as the mixing height (MH). The diagnosed MH for the YSU and the MYJ simulations will be denoted with $z_{i,ysu}$ (corresponding to $z_{i,truth}$ in the pseudo-data experiment) and $z_{i,myj}$ ($z_{i,model}$) respectively.

ACPD
11, 28169–28217, 2011

3 Results

3.1 Simulated mixing heights

In this section we present differences in diagnosed mixing heights between the two WRF simulations. Point comparisons are shown for 12 grid cells that contain the locations of observation sites continuously measuring CO_2 in Fig. 7. As observed concentrations from these sites are used in inversions, model errors in representing the vertical mixing at these sites directly influences flux estimates. These sites are placed throughout the simulation domain (marked with squares in Fig. 1). We also show results for all land cells in the domain (Fig. 8 a and b). The bias is calculated by time averaging the MH differences ($\langle z_{i,\mathrm{myj}} - z_{i,\mathrm{ysu}} \rangle$).

For the selected sites the bias is typically in the range of 200–400 m (~30–60 % relative to YSU, Fig. 7). The relative bias is higher in the nighttime and decreases as the ML deepens. During night in more than one third of the cases the MYJ MH equals 0 m (for further analysis the MH was set to 20 m which equals approximately half the height of the first vertical layer). This indicates very weak turbulence, i.e. TKE was falling below the threshold of 0.4 m s^{-2} as mentioned in Appendix A, leading to the rather large bias during nighttime when the YSU scheme produced on average heights of 300 m.

Timing of the mixed layer growth is generally in good agreement. However, a closer look at some sites reveals 1–2 h timing differences regarding the maximum MH, i.e. MYJ ML reaches the maximum earlier (e.g. SCH, BIK) and in most cases turbulence in MYJ ceases earlier in the afternoon (e.g. BIK, PDM). We also found higher growth rates in the morning for MYJ, i.e. averaged from 00:00 UTC to the time of maximum MH, MYJ MH grows for most sites 1–2 % of maximum MH per hour faster than YSU.

An example of the spatial patterns of bias during day and nighttime is shown in Fig. 8a and b. The spatial distribution of bias reveals larger bias during daytime over elevated terrain (e.g. Alps region) and a north-south gradient is visible. Compared to MYJ the YSU MH were usually much deeper over ocean which seems to affect the

ACPD
11, 28169–28217, 2011

bias in maritime areas, e.g. deeper YSU MLH advected over British Isles and coast of France during nighttime. The bias standard deviation is usually in the ranges 150–200 m (night time) and 350–450 m (daytime).

In summary, a general underestimation of MYJ MH by 30 % (~500 m) during daytime and at least a factor of two larger during nighttime (~150 m) is evident. A finding that is in line with previous studies showing that Mellor-Yamada based schemes tend to produce less turbulence than comparable PBL parameterizations (e.g. Sun and Ogura, 1980; Janjic, 2002; Steeneveld et al., 2008; Nakanishi and Niino, 2009; Hu et al., 2010).

These results confirm the initial assumption of quite noticeable differences in vertical mixing between both schemes with much lower MH in MYJ in line with the considerations in the 1-D conceptual model (Sect. 2.3). Rather different from the conceptual model is the diurnally varying bias in the WRF simulations (roughly 30 % daytime, 60 % nighttime) whereas in the 1-D case we assumed a constant 30 % low bias of MH. In our numerical experiment this time varying MH bias combined with the sign reversal of surface fluxes can lead to a strong diurnal rectifier effect. In the following section the impact on simulated CO_2 fields will be presented.

3.2 CO_2 mismatch

Here we show the bias in simulated CO_2 and the bias reduction after applying the reshuffling method (Eq. 2) to each land pixel and the full simulation period of the MYJ fields. The correction is applied offline (after the simulation has finished) to the hourly model output. For the reshuffling method we computed averaged ML concentration by integrating over all n vertical model levels below the diagnosed MH, i.e. $C_m = \sum_{i=1}^{n} m_i C_i / \sum_{i=1}^{n} m_i$ where m_i is mass and C_i the CO_2 mixing ratio of grid cell i. In case MH was below 20 m we used half the height of the first model level instead. We will refer to these ML averaged mixing ratios in the following as $C_{m,ysu}$ and $C_{m,myj}$ respectively. Note, the reshuffling is a local method (1-D) and thus applied on a per pixel basis, which neither gets any information from surrounding grid cells (space and time) nor does it affect them. Similar to the previous section we show the results for the selected sites and the entire simulation domain.

ACPD
11, 28169–28217, 2011

Figure 9 shows the average diurnal variation of the CO_2 mismatch, i.e. the bias at each of the 12 grid cells containing the observation sites. Similar to the conceptual model experiment we estimate the CO_2 mismatch by computing the differences $C_{m,myj} - C_{m,ysu}$. The bias is determined as time mean of these differences ($\langle C_{m,myj} - C_{m,ysu} \rangle$ and the random error refers to the standard deviation sd($C_{m,myj} - C_{m,ysu}$)). The course of the bias over 24 h (monthly mean diurnal variation of the mismatch) reflects the combined effect of the discrepancies in the simulated MH and the dominating direction of the surface fluxes (night CO_2 release, day CO_2 uptake) at these sites with much larger bias during nighttime (typically 4 to 10 ppm) than daytime (−3 to −1 ppm).

A large span of the bias is related to differences in timing of growth (morning) and decay (afternoon) of the mixed layer and the general weak mixing in MYJ during stable conditions. For instance the high altitude station Pic Du Midi has a negative peak (−6 ppm) at 10:00 local time (LT) and another one at 19:00 LT which are dominated by the MYJ CO_2 PBL concentration (not shown). A higher MYJ ML growth rate can be seen at PDM (cf. Fig. 7). In this case the maximum height is for both schemes around 13:00 LT, but in YSU deepening of the mixed layer starts earlier (YSU: 05:00 LT, MYJ: 09:00 LT) and is at that time already at 20 % of the maximum height (MYJ 09:00 LT at 5 %). NEE at PDM becomes dominated by photosynthesis around 07:00 LT (not shown) about 2 h before mixing starts to increase in MYJ, thus MYJ CO_2 mixing ratio is dropping much faster. Later in the morning a change of CO_2 concentration is caused by entrainment with air above the mixed layer. At 10:00 LT when the MYJ z_i growth rate is at maximum (MYJ: 30 % of maximum z_i per hour) this entrainment flux is dominating the photosynthesis flux and causes the CO_2 concentration to rise, because the air above the fast growing ML has relatively higher CO_2 concentration. Sudden bias increases in the late afternoon are caused by fast decaying turbulence in the MYJ simulation while the photosynthesis is still dominating fluxes for 1–2 h (cf. PDM 19:00 LT, Fig. 9).

ACPD
11, 28169–28217, 2011

The comparably large night bias at Cabauw is caused by firstly a larger bias in MH which is in the early morning (01:00–05:00 LT) between 300 and 400 m whereas bias at all the other sites in the range of 200 to 300 m (cf. Fig. 7), second and more importantly the larger influence of anthropogenic emissions (contribution to surface CO_2 at CBW between 01:00–07:00 LT above 25 ppm in MYJ, all other sites below 5 ppm).

To summarize the effect of the reshuffling method (Eq. 2) we report the bias reduction which is calculated as the relative difference of the absolute bias before and after applying the correction:

$$\text{bias reduction} = \frac{\left|\left\langle C_{\text{m,myj}} - C_{\text{m,ysu}} \right\rangle\right| - \left|\left\langle C_{\text{m,corrected}} - C_{\text{m,ysu}} \right\rangle\right|}{\left|\left\langle C_{\text{m,myj}} - C_{\text{m,ysu}} \right\rangle\right|} \times 100 \quad (5)$$

Thus, a perfect correction would yield a bias reduction of 100 %.

The bias after applying the correction (Eq. 2) is reduced substantially for all stations (Fig. 9). During daytime the bias is reduced 60–90 % (Fig. 10a) for most stations. Throughout the domain the bias is mostly reduced for night and day time (shown in Fig. 11). During nighttime MYJ concentration is much higher, consistent with the very shallow ML (30 % of land pixels in the 1st model layer about 20 m a.g.l. for YSU the same is true for less than 1 %) and the net release of CO_2. The correlation of the temporal evolution of the ML CO_2 between both simulations is high (70–80 %, Fig. 10c) and the corrected fields can not improve this correlation.

The bias pattern is mainly controlled by the surface fluxes and the orography. On the one hand in areas where surface fluxes are weak the CO_2 bias is smaller and on the other hand mixing increases in MYJ over areas with elevated terrain (enhanced heat flux and surface friction) to heights closer to YSU (Fig. 8a, e.g. Alps, Pyrenees, Scottish Highlands, Anatolia) causing the bias to decrease as well.

The daytime (11:00–14:00 UTC) bias for all land pixels is usually in the range of 3 ppm before and 1 ppm after applying the correction. Standard deviations of the bias are generally in range of 1 to 3 ppm during daytime and more than a factor of two larger during nighttime (01:00–04:00 UTC, not shown).

ACPD
11, 28169–28217, 2011

This spatially and temporally consistent bias clearly shows the sensitivity of simulated diurnal variation of mixed layer CO_2 to the choice of the PBL parameterization in highly resolved transport models.

Figure 12 summarizes the reshuffling performance for each land pixels and hour of the day by averaging the bias (a) and its standard deviation (b) spatially. Like the bias, the random error (standard deviation of bias) is reduced, albeit at much lower rates of 10–20 % during daytime, and 30–40 % during nighttime (Fig. 12b) when the CO_2 mismatch is spatially more uniformly distributed (cf. Fig. 11a and c) and thus conceptual deficiencies (i.e. 1-D correction of the 3-D simulation) of the correction seem to play a minor role compared to daytime (more on this in the discussion section).

In summary, we conclude that the overall effect of the reshuffling is a substantial improvement in the diurnal amplitude of MYJ ML CO_2.

Obviously the performance of the correction breaks down during transition times of ML development, i.e. during morning growth and during afternoon when turbulence ceases (cf. Fig. 10 ORL, OXK and Fig. 12). The reason for this effect is twofold: (1) the bias contains two flux regimes (release, uptake), resulting in a sign change of the CO_2 mismatch. The incoming solar radiation causes the transition from one regime to the other (sunrise and sunset). At these transition times the bias approaches 0 ppm and thus the reshuffling method has on average a minor effect or even increases the CO_2 mismatch (cf. Sect. 2.3, Fig. 3b 5–9 h and 18–20 h). (2) Inconsistencies between the CO_2 profiles and the diagnosed mixing height. For instance we often found during morning growth the ML was clearly evident from the simulated CO_2 profiles (well mixed in the first several model layers) while the diagnosed MH was for both simulations near 20 m (somewhere in the ML instead at the top of it). As a consequence the correction had almost no effect ($z_{i,\mathrm{model}}/z_{i,\mathrm{truth}} \approx 1$ in Eq. 2). This is reflected in Fig. 9 e.g. at the stations Fyodorovskoje (07:00–10:00 LT), Ochsenkopf (10:00–12:00 LT), Puy De Dome (07:00–10:00 LT).

For MYJ a reason for MH/CO_2 inconsistencies might be a too large TKE threshold (cf. Sect. 2.4), which can lead to diagnosed MH that are lower than gradients in the

ACPD
11, 28169–28217, 2011

vertical profiles of the simulated scalars themselves suggest (Hu et al., 2010). YSU, on the other hand, uses a bulk Richardson method to diagnose z_i that is very sensitive to the choice of the critical Richardson number (Ri_c, cf. Appendix A). This resulted in large fluctuations (several 100 m) in z_i time series especially during transition times (well mixed to stable and vice versa) when Ri_c changes from 0 to 0.25 (Hong, 2007). The fluctuation were not reflected in the CO_2 profiles as they don't seem to adapt quickly to sudden MH changes. In such cases the concentration gradient in the CO_2 profile between the MH and the layer above would be a better diagnostic for the MH. But as stated in Sect. 2.4 this information is usually not available.

These results highlight the dependence of the correction on a method that accurately estimates the effective mixed layer height. Other reasons for such inconsistency can be related to conceptual deficiencies of the reshuffling method and are discussed further in the following section.

4 Discussion

The results support the initial hypothesis that the diurnal CO_2 bias is to a first order controlled by local differences in vertical mixing and that these differences are reflected in the mixing layer heights. With our rather indirect reshuffling method the gain in information represented by the known MH could be translated to a reduced bias in tracer space. These findings underline the potential to successfully constrain the transport model by assimilating observation based mixing heights. This would improve convective tendencies directly. But probably more importantly such approaches can lead to improvements of the respective PBL parameterization and thus enhanced process understanding. Ways to assimilate mixing height data are currently explored (McGrath-Spangler and Denning, 2010).

Regarding the presented reshuffling method, not all of the bias is explained and random error is only slightly improved. This result comes as no surprise, as the 1-D correction neglects changes in the column due to horizontal advection (cf. Sect. 2.3). Thus

ACPD
11, 28169–28217, 2011

the reshuffling method can not account for errors that arise from differences in horizontal transport of CO_2. Such differences can include (1) horizontal advection within the mixed layer, (2) deep cumulus convection combined with high altitude horizontal winds, and (3) wind shear above the nighttime SBL.

To investigate the effect of these different causes we analyzed the simulation fields to find situations in which the correction fails. For simplicity we define failure of the correction as cases when the absolute CO_2 error after applying the correction is significantly larger than before:

$$\left|C_{\mathrm{m,corrected}} - C_{\mathrm{m,ysu}}\right| - \left|C_{\mathrm{m,myj}} - C_{\mathrm{m,ysu}}\right| \; > \; 1\,\mathrm{ppm}$$

As example we show in Fig. 13a a map for 10 August of the simulation period where each pixel that is classified as failure is marked. Possible reasons for these apparent inconsistencies are (1) the diagnosed MH does not represent the effective top of the ML (cf. previous section) (2) the CO_2 fluxes into the model column are different for YSU and MYJ. To circumvent the first trivial cause for failure one can either try to improve the methods to diagnose the MLH correctly or choose one from a set of available methods that is better suited for the current synoptic condition, which is still a matter of ongoing research (Seibert et al., 2000).

The second source of failure, which is related to conceptual deficiencies of the reshuffling method, seems to be closely related to differences in the convective tendencies that are calculated within the PBL scheme. For illustration, Fig. 13b and c shows the Potential Available Convective Energy (CAPE). Although both simulations use the same cumulus parameterization (Table 1) CAPE differs substantially near areas where correction consistently fails (arrows in Fig. 13). For these areas mass fluxes into the cloud base and vertical velocities are considerably higher in the MYJ simulation (not shown). This suggest that the CO_2 signature within the ML is transported to higher altitudes differently in both simulations. Because above the ML wind shear is likely to occur and wind speed increases from subgeostrophic within the ML to geostrophic above, differences in vertical transport of mass also leads to altered horizontal trajectories of the CO_2 molecules. Therefore, tracer transport might be more local in one

ACPD
11, 28169–28217, 2011

simulation than in the other causing greater errors in 1-D budgets in columns downstream, because these mass contributions by advection are neglected.

To account for the effects of such synoptic events one could think of a correction method that tracks cumulus mass fluxes and calculates particle trajectories e.g. using lagrangian transport models. This information could then be used with an enhanced budget formulation which includes terms for horizontal advection (e.g. Aubinet et al., 2005a). But to employ such a method in an inversion system seems practically unfeasible. Thus, assimilation approaches like 3D/4DVAR or Extended Kalman Filters that use observation based MH to optimize the model-state for tracer transport seem preferable.

However, our results give reason to hope that already a relatively simple correction can help to improve the flux estimates of regional inversions:

1. The derived model-data mismatch statistics (error covariances) can be propagated through the inversion system as demonstrated by G08. This approach estimates posterior flux uncertainties that are more consistent with the truth, which is the basis for any reliable model-data fusion system (Gerbig et al., 2009).

2. Observation based mixing heights could be used to constrain the simulated CO_2 fields by applying the introduced reshuffling method before cost functions in the inversion framework are minimized. In combination with the before mentioned error propagation to account for the remaining CO_2 mismatch this can lead to improved posterior uncertainties and flux estimates.

Basis for any of these methods to improve regional inversions are reliable estimates of the mixing heights from observations of the atmospheric state. Mixing heights can be obtained from several observational sources, in-situ measurements like radio soundings (G08, Seibert et al., 2000; Seidel et al., 2010) and a variety of acoustic, electro-magnetic and optical remote sensing techniques, like SODAR (Sonic Detecting And Ranging), RADAR (Radio Detection and Ranging) (Emeis et al., 2004). Aerosol backscatter profiles measured by LIDARs (LIght Detection And Ranging) and

ACPD
11, 28169–28217, 2011

ceilometers combined with sophisticated retrieval algorithms can provide MH estimates as well. Especially ceilometers, originally designed to detect cloud bases, promise a relatively cheap and easy to deploy method to acquire large quantities of such data and thus being discussed to be part of measurement frameworks like the Integrated Carbon Observation System (Haeffelin et al., 2011; Milroy et al., 2011; http://www.icos-infrastructure.eu/). A number of ceilometer networks are operated by weather services throughout Europe[2]. For example, 36 sites of the German weather service (DWD) were recently used in the study of Flentje et al. (2010) to measure the volcanic ash plume of the 2010 Eyjafjallajökull eruption.

Another promising source of data can be obtained from satellites like CALIPSO (Cloud-Aerosol LIDAR and Infrared Pathfinder Satellite Observations). Similar to ground-based ceilometers they provide aerosol backscatter profiles of the atmosphere that can be used together with sophisticated retrieval algorithms to infer mixing heights (Jordan et al., 2010). The advantage of such satellite observations is a dense spatio-temporal coverage which can complement the other mentioned data streams to constrain transport over large areas.

5 Conclusions

In this study we presented results from a synthetic experiment using the atmospheric transport model WRF coupled to the diagnostic biosphere model VPRM and anthropogenic emissions to realistically simulate transport of CO_2 for large parts of the European continent at 10 km horizontal resolution. To elucidate the impact of uncertainties in vertical mixing on modeled CO_2 transport, we simulated the period of August 2006 with different commonly used parameterizations of the PBL (YSU and MYJ), while keeping CO_2 fluxes the same. We used diagnosed mixed layer heights of the modeled meteorology to quantify differences in vertical mixing strength between both simula-

[2]Denmark, Great Britain, France, Germany, the Netherlands, Iceland, Sweden, Switzerland

ACPD
11, 28169–28217, 2011

tions. A reshuffling method to relate differences in mixing height to resulting differences (errors) in CO_2 was presented. The method was tested with a conceptual 1-D model (neglecting horizontal advection) and with the complex 3-D WRF simulations.

Following the initial questions of this paper, the main results are:

1. We found significant differences in simulated mixing heights in amplitude, which were in the general range of 30–40 % relative to YSU mixing heights for daytime and factor of two larger for nighttime. The MYJ ML often developed later in the morning and turbulence ceased earlier as in the YSU simulation (time lags of 1–2 h).

2. The simulated diurnal cycle of mixed layer CO_2 mole fractions differed considerably in amplitude during daytime (1–3 ppm differences) and even more during nighttime (4–10 ppm differences), with standard deviations in the same order. Both simulations agreed well in phasing (r squared ~0.8). However, large peaks in bias were found in point comparisons (grid cells including observational sites) related to timing differences of turbulence (−6 ppm during daytime) as well as influence of nearby anthropogenic emission sources (Cabauw, 30 ppm nighttime).

3. The reshuffling method (Eq. 2) substantially reduced the bias in mixed layer CO_2 by 70–80 % during daytime (>80 % nighttime), when using information about the true mixing height (YSU). This result underlines the potential of observation based mixing height data to constrain transport in order to improve regional surface-atmosphere flux estimates by CO_2 inversions. Failure of our simple correction method was shown to be due to inconsistencies in methods to diagnose mixing heights, and to conceptual deficiencies related to neglecting the horizontal advection. More sophisticated ways to assimilate mixing height data are needed to gain process understanding of PBL dynamics in order to improve PBL parameterizations.

We conducted an idealized experiment with two different PBL parameterizations. So one can question if the mismatches found in MH and CO_2 concentration are an realistic

ACPD
11, 28169–28217, 2011

estimate of the true uncertainty. However, we would like to stress that both PBL parameterizations are commonly used and several studies validated these schemes in combination with WRF against meteorological observations clearly showing their ability to realistically simulate PBL dynamics in different seasonal and synoptic conditions (e.g. Borge et al., 2008; Hu et al., 2010). In this regard our study underlines the need to further investigate transport errors in vertical mixing to infer reliable regional flux estimates. Independent from the absolute values of model error, the presented concept can be used to infer vertical transport error statistics that can be propagated through inversions. In addition, a direct application of the reshuffling method presented in this paper to reduce the CO_2 model-data mismatch prior to the flux optimization will be tested in future inversion studies. Observation based mixing heights to constrain transport will be obtained from radiosondes, ceilometers or satellites.

Future work should also comprise ensemble simulations with a broader range of model/PBL scheme combinations for different seasons and years. Beside CO_2 these studies should include other GHG like CH_4 and N_2O. Observations of trace gases like SF_6 and ^{222}Rn with known surface fluxes could be used to isolate vertical transport mismatches from other error sources (G08). For the advantage of these efforts a closer collaboration with experts from weather services and numerical weather prediction centers should be fostered.

Appendix A

Summary of the PBL parameterizations

In this section we give a brief summary of the main characteristics and differences of both PBL schemes. Most relevant to this study are the linkage of PBL parameterization and CO_2 transport and the determination of the PBL height within the schemes.

To allow for coupling to several PBL schemes in WRF-Chem the change of the CO_2 mixing ratio (C) due to turbulent vertical mixing in a column of air is parameterized with

ACPD
11, 28169–28217, 2011

the heat exchange coefficient K_h in a first order closure to calculate the covariances $-\overline{w'C'}$ as a function of the height above the surface z as in Grell et al. (2000):

$$-\overline{w'C'} = K_h \times \frac{\partial C}{\partial z} \tag{A1}$$

Assuming that the turbulent transport of heat is equally acting on the tracer transport and neglecting non-local mixing in case of large eddies. The exchange coefficient links turbulent tracer transport to the PBL schemes which determine K_h not only for the PBL but for the whole atmospheric column.

The YSU PBL scheme is a first order K-profile model it calculates the exchange coefficient for momentum K_m and from that derives K_h using the relationship to the Prandtl number Pr for the mixed layer Hong et al. (2006):

$$K_m = k w_s z \times (1 - \frac{z}{h})^p, \tag{A2}$$

$$K_h = K_m / Pr \tag{A3}$$

Where $k = 0.4$ is the von Kármán constant, h is the top of the PBL, $p = 2$ is the profile shape exponent and w_s is the mixed layer velocity scale which is derived from the convective velocity scale (w_*), the wind profile and the surface friction velocity (u_*). Above the top of the PBL Pr and the coefficients are calculated differently according to the stability of the atmosphere. In the YSU scheme the PBL height is defined as the level of minimum heat flux, computed as the height where the bulk Richardson number Ri gets larger than a prescribed threshold (critical bulk Richardson number Ri_c). Ri is obtained from the virtual potential temperature (Θ_v), wind speed (U) profiles, the surface temperature (Θ_s), the virtual potential temperature at the lowest model level (Θ_{va})

$$Ri(z) = \frac{g(\Theta_v(z) - \Theta_s)z}{\Theta_{va} U(z)^2} \tag{A4}$$

ACPD
11, 28169–28217, 2011

Ri_c is set to 0 in unstable and 0.25 in stable conditions over land, which is diagnosed in an iterative manner based on the calculated profile of Richardson numbers (Hong, 2007).

In contrast the MYJ PBL is a 2.5 order local closure scheme which solves the budget equation for TKE ($TKE = (u'^2 + v'^2 + w'^2)/2$). The heat exchange coefficient is derived from

$$K_h = l \times S_H \times \sqrt{2TKE} \tag{A5}$$

S_H being a complex algebraic function of Ri which is constraint by several empirical constants. A key quantity in TKE models is the master length scale or mixing length l, in the MYJ scheme the diagnostic formula of Janjic (2002) is used for the PBL:

$$l = l_0 \times \frac{kz}{(kz + l_0)}, \tag{A6}$$

$$l_0 = \alpha \frac{\int_0^h |z| \times \sqrt{2 \times TKE}\, dz}{\int_0^h \sqrt{2 \times TKE}\, dz}, \; \alpha = 0.25 \tag{A7}$$

Here the PBL height h is defined as the lowest level above the surface where TKE reaches its maximum and decreases with height and using 5000 m as upper limit. If the TKE is dropping below the limit of 0.4 m s^{-2}, h is set to 0 m.

Acknowledgements. The authors would like to thank the Max Planck Society for providing funding and facilities, Steven Wofsy for helping with the conceptual model, Christian Rödenbeck, Ravan Ahmadov, Veronika Beck and Dhanya K. Pillai for general discussions and help, the IT department of the Max Planck Institute for Biogeochemistry for technical aid and Kai Uwe Totsche for his constructive support of this work.

The service charges for this open access publication have been covered by the Max Planck Society.

ACPD
11, 28169–28217, 2011

References

Ahmadov, R., Gerbig, C., Kretschmer, R., Körner, S., Neininger, B., Dolman, A. J., and Sarrat, C.: Mesoscale covariance of transport and CO_2 fluxes: Evidence from observations and simulations using the WRF-VPRM coupled atmosphere-biosphere model, J. Geophys. Res.-Atmos., 112, D22107, doi:10.1029/2007JD008552, 2007. 28171, 28173, 28174, 28175, 28176, 28179

Ahmadov, R., Gerbig, C., Kretschmer, R., Körner, S., Rödenbeck, C., Bousquet, P., and Ramonet, M.: Comparing high resolution WRF-VPRM simulations and two global CO_2 transport models with coastal tower measurements of CO_2, Biogeosciences, 6, 807–817, doi:10.5194/bg-6-807-2009, 2009. 28173, 28176

Aubinet, M., Berbigier, P., Bernhofer, C. H., Cescatti, A., Feigenwinter, C., Granier, A., Grünwald, T. H., Havrankova, K., Heinesch, B., Longdoz, B., Marcolla, B., Montagnani, L., and Sedlak, P.: Comparing CO_2 storage and advection conditions at night at different carboeuroflux sites, Bound.-Lay. Meteorol., 116, 63–94, 2005a. 28178, 28190

Aubinet, M., Heinesch, B., Perrin, D., and Moureaux, C.: Discriminating net ecosystem exchange between different vegetation plots in a heterogeneous forest, Agr. Forest Meteorol., 132, 315–328, 2005b. 28172

Aulagnier, C., Rayner, P., Ciais, P., Vautard, R., Rivier, L., and Ramonet, M.: Is the recent build-up of atmospheric CO_2 over Europe reproduced by models. Part 2: an overview with the atmospheric mesoscale transport model CHIMERE, Tellus B, 62, doi:10.1111/j.1600-0889.2009.00443.x, 2010. 28173

Bakwin, P. S., Davis, K. J., Yi, C., Wofsy, S. C., Munger, J. W., Haszpra, L., and Barcza, Z.: Regional carbon dioxide fluxes from mixing ratio data, Tellus B, 56, 301–311, 2004. 28172

Borge, R., Alexandrov, V., del Vas, J. J., Lumbreras, J., and Rodriguez, E.: A comprehensive sensitivity analysis of the WRF model for air quality applications over the Iberian Peninsula, Atmos. Environ., 42, 8560–8574, doi:10.1016/j.atmosenv.2008.08.032, 2008. 28173, 28193

Canadell, J. G., Le Qur, C., Raupach, M. R., Field, C. B., Buitenhuis, E. T., Ciais, P., Conway, T. J., Gillett, N. P., Houghton, R. A., and Marland, G.: Contributions to accelerating atmospheric CO_2 growth from economic activity, carbon intensity, and efficiency of natural sinks, P. Natl. Acad. Sci. USA, 104, 18866–18870, 2007. 28170

Chou, W. W., Wofsy, S. C., Harriss, R. C., Lin, J. C., Gerbig, C., and Sachse, G. W.: Net fluxes of CO_2 in Amazonia derived from aircraft observations, J. Geophys. Res.-Atmos., 107, 4614,

ACPD
11, 28169–28217, 2011

doi:10.1029/2001JD001295, 2002. 28172, 28178
Denning, A., Fung, I., and Randall, D.: Latitudinal gradient of atmospheric CO_2 due to seasonal exhchange with land biota, Nature, 376, 240–243, 1995. 28171
Denning, A. S., Randall, D. A., Collatz, G. J., and Sellers, P. J.: Simulations of terrestrial carbon metabolism and atmospheric CO_2 in a general circulation model. 2. Simulated CO_2 concentrations, Tellus B, 48, 543–567, 1996. 28171, 28173
Denning, A. S., Takahashi, T., and Friedlingstein, P.: Can a strong atmospheric CO_2 rectifier effect be reconciled with a "reasonable" carbon budget?, Tellus B, 51, 249–253, 1999. 28171
Denning, A. S., Zhang, N., Yi, C. X., Branson, M., Davis, K., Kleist, J., and Bakwin, P.: Evaluation of modeled atmospheric boundary layer depth at the WLEF tower, Agr. Forest Meteorol., 148, 206–215, 2008. 28171, 28173
Dolman, A. J., Noilhan, J., Durand, P., Sarrat, C., Brut, A., Piguet, B., Butet, A., Jarosz, N., Brunet, Y., Loustau, D., Lamaud, E., Tolk, L., Ronda, R., Miglietta, F., Gioli, B., Magliulo, V., Esposito, M., Gerbig, C., Körner, S., Glademard, R., Ramonet, M., Ciais, P., Neininger, B., Hutjes, R. W. A., Elbers, J. A., Macatangay, R., Schrems, O., Pérez-Landa, G., Sanz, M. J., Scholz, Y., Facon, G., Ceschia, E., and Beziat, P.: The CarboEurope regional experiment strategy, B. Am. Meteorol. Soc., 87, 1367–1379, 2006. 28179
Emeis, S., Münkel, C., Vogt, S., Müller, W. J., and Schäfer, K.: Atmospheric boundary-layer structure from simultaneous SODAR, RASS, and ceilometer measurements, Atmos. Environ., 38, 273–286, 2004. 28190
Flentje, H., Claude, H., Elste, T., Gilge, S., Köhler, U., Plass-Dülmer, C., Steinbrecht, W., Thomas, W., Werner, A., and Fricke, W.: The Eyjafjallajökull eruption in April 2010 – detection of volcanic plume using in-situ measurements, ozone sondes and lidar-ceilometer profiles, Atmos. Chem. Phys., 10, 10085–10092, doi:10.5194/acp-10-10085-2010, 2010. 28191
Gerbig, C., Lin, J. C., Wofsy, S. C., Daube, B. C., Andrews, A. E., Stephens, B. B., Bakwin, P. S., and Grainger, C. A.: Toward constraining regional-scale fluxes of CO2 with atmospheric observations over a continent: 1. Observed spatial variability from airborne platforms, J. Geophys. Res.-Atmos., 108, 4756, doi:10.1029/2002JD003018, 2003. 28171
Gerbig, C., Körner, S., and Lin, J. C.: Vertical mixing in atmospheric tracer transport models: error characterization and propagation, Atmos. Chem. Phys., 8, 591–602, doi:10.5194/acp-8-591-2008, 2008. 28171, 28173
Gerbig, C., Dolman, A. J., and Heimann, M.: On observational and modelling strategies targeted at regional carbon exchange over continents, Biogeosciences, 6, 1949–1959,

ACPD
11, 28169–28217, 2011

doi:10.5194/bg-6-1949-2009, 2009. 28171, 28190
Gibert, F., Schmidt, M., Cuesta, J., Ciais, P., Ramonet, M., Xueref, I., Larmanou, E., and Flamant, P. H.: Retrieval of average CO_2 fluxes by combining in situ CO_2 measurements and backscatter lidar information, J. Geophys. Res.-Atmos., 112, D10301, doi:10.1029/2006JD008190, 2007. 28172, 28179
Göckede, M., Michalak, A. M., Vickers, D., Turner, D. P., and Law, B. E.: Atmospheric inverse modeling to constrain regional scale CO_2 budgets at high spatial and temporal resolution, J. Geophys. Res., 115, D15113, doi:10.1029/2009JD012257, 2010. 28171
Grell, G., Emeis, S., Stockwell, W., Schoenemeyer, T., Forkel, R., Michalakes, J., Knoche, R., and Seidl, W.: Application of a multiscale, coupled MM5/chemistry model to the complex terrain of the VOTALP valley campaign, Atmos. Environ., 34, 1435–1453, 2000. 28194
Grell, G., Peckham, S., Schmitz, R., McKeen, S., Frost, G., Skamarock, W., and Eder, B.: Fully coupled "online" chemistry within the WRF model, Atmos. Environ., 39, 6957–6975, doi:10.1016/j.atmosenv.2005.04.027, 2005. 28175
Gurney, K. R., Law, R. M., Denning, A. S., Rayner, P. J., Baker, D., Bousquet, P., Bruhwiler, L., Chen, Y.-H., Ciais, P., Fan, S., Fung, I. Y., Gloor, M., Heimann, M., Higuchi, K., John, J., Maki, T., Maksyutov, S., Masarie, K., Peylin, P., Prather, M., Pak, B. C., Randerson, J., Sarmiento, J., Taguchi, S., Takahashi, T., and Yuen, C.-W.: Towards robust regional estimates of CO_2 sources and sinks using atmospheric transport models, Nature, 415, 626–630, 2002. 28171
Haeffelin, M., Angelini, F., Morille, Y., Martucci, G., Frey, S., Gobbi, G., Lolli, S., O'Dowd, C., Sauvage, L., Xueref-Rémy, I., Wastine, B., and Feist, D.: Evaluation of Mixing-Height Retrievals from Automatic Profiling Lidars and Ceilometers in View of Future Integrated Networks in Europe, Bound.-Lay. Meteorol., 1–27, doi:10.1007/s10546-011-9643-z, 2011. 28191
Heimann, M. and Reichstein, M.: Terrestrial ecosystem carbon dynamics and climate feedbacks, Nature, 451, 289–292, 2008. 28170
Helliker, B. R., Berry, J. A., Betts, A. K., Bakwin, P. S., Davis, K. J., Denning, A. S., Ehleringer, J. R., Miller, J. B., Butler, M. P., and Ricciuto, D. M.: Estimates of net CO_2 flux by application of equilibrium boundary layer concepts to CO_2 and water vapor measurements from a tall tower, J. Geophys. Res.-Atmos., 109, D20106, doi:10.1029/2004JD004532, 2004. 28172, 28178
Hong, S.-Y.: Stable Boundary Layer Mixing in a Vertical Diffusion Scheme, in: Fall conference of the Korea Meteor. Soc., Seoul, Korea, 2007. 28188, 28195

ACPD
11, 28169–28217, 2011

Hong, S.-Y., Noh, Y., and Dudhia, J.: A new vertical diffusion package with an explicit treatment of entrainment processes, Mon. Weather Rev., 134, 2318–2341, 2006. 28173, 28194

Houweling, S., Aben, I., Breon, F.-M., Chevallier, F., Deutscher, N., Engelen, R., Gerbig, C., Griffith, D., Hungershoefer, K., Macatangay, R., Marshall, J., Notholt, J., Peters, W., and Serrar, S.: The importance of transport model uncertainties for the estimation of CO_2 sources and sinks using satellite measurements, Atmos. Chem. Phys., 10, 9981–9992, doi:10.5194/acp-10-9981-2010, 2010. 28171

Hu, X.-M., Nielsen-Gammon, J. W., and Zhang, F.: Evaluation of Three Planetary Boundary Layer Schemes in the WRF Model, J. Appl. Meteorol. Clim., 49, 1831–1844, doi:10.1175/2010JAMC2432.1, 2010. 28174, 28182, 28184, 28188, 28193

IPCC: Climate Change 2007: Synthesis Report. Contribution of Working Groups I, II and III to the Fourth Assessment Report of the Intergovernmental Panel on Climate Change, edited by: Core Writing Team, Pachauri, R. K., and Reisinger, A., IPCC, Cambridge University Press, Cambridge, 2007. 28170

Janjic, Z. I.: Nonsingular Implementation of the MellorYamada Level 2.5 Scheme in the NCEP Meso model, Office Note 437, NCEP Office, 61 pp., 2002. 28173, 28184, 28195

Jordan, N. S., Hoff, R. M., and Bacmeister, J. T.: Validation of Goddard Earth Observing System-version 5 MERRA planetary boundary layer heights using CALIPSO, J. Geophys. Res.-Atmos., 115, D24218, doi:10.1029/2009JD013777, 2010. 28191

Jung, M., Henkel, K., Herold, M., and Churkina, G.: Exploiting synergies of global land cover products for carbon cycle modeling, Remote Sens. Environ., 101, 534–553, 2006. 28175

Karstens, U., Gloor, M., Heimann, M., and Rödenbeck, C.: Insights from simulations with high-resolution transport and process models on sampling of the atmosphere for constraining midlatitude land carbon sinks, J. Geophys. Res.-Atmos., 111, D12301, doi:10.1029/2005JD006278, 2006. 28171

Laubach, J. and Fritsch, H.: Convective boundary layer budgets derived from aircraft data, Agr. Forest Meteorol., 111, 237–263, 2002. 28172, 28178

Lauvaux, T., Pannekoucke, O., Sarrat, C., Chevallier, F., Ciais, P., Noilhan, J., and Rayner, P. J.: Structure of the transport uncertainty in mesoscale inversions of CO_2 sources and sinks using ensemble model simulations, Biogeosciences, 6, 1089–1102, doi:10.5194/bg-6-1089-2009, 2009. 28171

Law, R. M., Rayner, P. J., Denning, A. S., Erickson, D., Fung, I. Y., Heimann, M., Piper, S. C., Ramonet, M., Taguchi, S., Taylor, J. A., Trudinger, C. M., and Watterson, I. G.: Variations in

ACPD
11, 28169–28217, 2011

modeled atmospheric transport of carbon dioxide and the consequences for CO_2 inversions, Global Biogeochem. Cy., 10, 783–796, 1996. 28171

Law, R. M., Matear, R. J., and Francey, R. J.: Saturation of the Southern Ocean CO_2 sink due to recent climate change, Science, 319, 570a–570a, 2008. 28171

Lin, J. C. and Gerbig, C.: Accounting for the effect of transport errors on tracer inversions, Geophys. Res. Lett., 32, L01802, doi:10.1029/2004GL021127, 2005. 28171

Mahadevan, P., Wofsy, S. C., Matross, D. M., Xiao, X., Dunn, A. L., Lin, J. C., Gerbig, C., Munger, J. W., Chow, V. Y., and Gottlieb, E. W.: A satellite-based biosphere parameterization for net ecosystem CO_2 exchange: Vegetation Photosynthesis and Respiration Model (VPRM), Global Biogeochem. Cy., 22, GB2005, doi:10.1029/2006GB002735, 2008. 28175

McGrath-Spangler, E. L. and Denning, A. S.: Impact of entrainment from overshooting thermals on land-atmosphere interactions during summer 1999, Tellus B, 62, 441–454, doi:10.1111/j.1600-0889.2010.00482.x, 2010. 28172, 28188

Houweling, S., Aben, I., Breon, F.-M., Chevallier, F., Deutscher, N., Engelen, R., Gerbig, C., Griffith, D., Hungershoefer, K., Macatangay, R., Marshall, J., Notholt, J., Peters, W., and Serrar, S.: The importance of transport model uncertainties for the estimation of CO_2 sources and sinks using satellite measurements, Atmos. Chem. Phys., 10, 9981–9992, doi:10.5194/acp-10-9981-2010, 2010. 28191

Nakanishi, M. and Niino, H.: Development of an Improved Turbulence Closure Model for the Atmospheric Boundary Layer, J Meteorol. Soc. Jpn., 87, 895–912, doi:10.2151/jmsj.87.895, 2009. 28184

Nisbet, E. and Weiss, R.: Top-Down Versus Bottom-Up, Science, 328, 1241–1243, doi:10.1126/science.1189936, 2010. 28171

Peters, W., Jacobson, A. R., Sweeney, C., Andrews, A. E., Conway, T. J., Masarie, K., Miller, J. B., Bruhwiler, L. M. P., Ptron, G., Hirsch, A. I., Worthy, D. E. J., van der Werf, G. R., Randerson, J. T., Wennberg, P. O., Krol, M. C., and Tans, P. P.: An atmospheric perspective on North American carbon dioxide exchange: CarbonTracker, P. Natl. Acad. Sci. USA, 104, 18925–18930, 2007. 28171

Pillai, D., Gerbig, C., Marshall, J., Ahmadov, R., Kretschmer, R., Koch, T., and Karstens, U.: High resolution modeling of CO_2 over Europe: implications for representation errors of satellite retrievals, Atmos. Chem. Phys., 10, 83–94, doi:10.5194/acp-10-83-2010, 2010. 28173, 28176

Pillai, D., Gerbig, C., Ahmadov, R., Rödenbeck, C., Kretschmer, R., Koch, T., Thompson, R.,

ACPD
11, 28169–28217, 2011

Neininger, B., and Lavrié, J. V.: High-resolution simulations of atmospheric CO_2 over complex terrain – representing the Ochsenkopf mountain tall tower, Atmos. Chem. Phys., 11, 7445–7464, doi:10.5194/acp-11-7445-2011, 2011. 28175, 28176

Pérez-Landa, G., Ciais, P., Gangoiti, G., Palau, J. L., Carrara, A., Gioli, B., Miglietta, F., Schumacher, M., Millán, M. M., and Sanz, M. J.: Mesoscale circulations over complex terrain in the Valencia coastal region, Spain – Part 2: Modeling CO_2 transport using idealized surface fluxes, Atmos. Chem. Phys., 7, 1851–1868, doi:10.5194/acp-7-1851-2007, 2007. 28173

Ramonet, M., Ciais, P., Aalto, T., Aulagnier, C., Chevallier, F., Cipriano, D., Conway, T. J., Haszpra, L., Kazan, V., Meinhardt, F., Paris, J.-D., Schmidt, M., Simmonds, P., Xueref-Rémy, I., and Necki, J. N.: A recent build-up of atmospheric CO_2 over Europe. Part 1: observed signals and possible explanations, Tellus B, 62, 1–13, doi:10.1111/j.1600-0889.2009.00442.x, 2009. 28173

Rödenbeck, C.: Estimating CO_2 sources and sinks from atmospheric mixing ratio measurements using a global inversion of atmospheric transport. Technical Report 6, Tech. rep., Max-Planck Institut für Biogeochemie, 2005. 28176

Rödenbeck, C., Houweling, S., Gloor, M., and Heimann, M.: CO_2 flux history 1982–2001 inferred from atmospheric data using a global inversion of atmospheric transport, Atmos. Chem. Phys., 3, 1919–1964, doi:10.5194/acp-3-1919-2003, 2003. 28171

Sarrat, C., Noilhan, J., Dolman, A. J., Gerbig, C., Ahmadov, R., Tolk, L. F., Meesters, A. G. C. A., Hutjes, R. W. A., Ter Maat, H. W., Pérez-Landa, G., and Donier, S.: Atmospheric CO_2 modeling at the regional scale: an intercomparison of 5 meso-scale atmospheric models, Biogeosciences, 4, 1115–1126, doi:10.5194/bg-4-1115-2007, 2007. 28173, 28176

Schimel, D. S., House, J. I., Hibbard, K. A., Bousquet, P., Ciais, P., Peylin, P., Braswell, B. H., Apps, M. J., Baker, D., Bondeau, A., Canadell, J., Churkina, G., Cramer, W., Denning, A. S., Field, C. B., Friedlingstein, P., Goodale, C., Heimann, M., Houghton, R. A., Melillo, J. M., Moore III, B., Murdiyarso, D., Noble, I., Pacala, S. W., Prentice, I. C., Raupach, M. R., Rayner, P. J., Scholes, R. J., Steffen, W. L., and Wirth, C.: Recent patterns and mechanisms of carbon exchange by terrestrial ecosystems, Nature, 414, 169–172, 2001. 28171

Seibert, P., Beyrich, F., Gryning, S.-E., Joffre, S., Rasmussen, A., and Tercier, P.: Review and intercomparison of operational methods for the determination of the mixing height, Atmos. Environ., 34, 1001–1027, 2000. 28189, 28190

Seidel, D. J., Ao, C. O., and Li, K.: Estimating climatological planetary boundary layer heights from radiosonde observations: Comparison of methods and uncertainty analysis, J. Geo-

ACPD
11, 28169–28217, 2011

phys. Res.-Atmos., 115, D1611, doi:10.1029/2009JD013680, 2010. 28190
Steeneveld, G. J., Mauritsen, T., de Bruijn, E. I. F., de Arellano, J. V.-G., Svensson, G., and Holtslag, A. A. M.: Evaluation of limited-area models for the representation of the diurnal cycle and contrasting nights in CASES-99, J. Appl. Meteorol. Clim., 47, 869–887, doi:10.1175/2007JAMC1702.1, 2008. 28184
Stephens, B., Wofsy, S., Keeling, R., Tans, P., and Potosnak, M.: The CO_2 budget and rectification airborne study: Strategies for measuring rectifiers and regional fluxes, in: Inverse Methods in Global Biogeochemical Cycles, vol. 114, 311–324, American Geophysical Union, 2000. 28171, 28178
Stephens, B. B., Gurney, K. R., Tans, P. P., Sweeney, C., Peters, W., Bruhwiler, L., Ciais, P., Ramonet, M., Bousquet, P., Nakazawa, T., Aoki, S., Machida, T., Inoue, G., Vinnichenko, N., Lloyd, J., Jordan, A., Heimann, M., Shibistova, O., Langenfelds, R. L., Steele, L. P., Francey, R. J., and Denning, A. S.: Weak northern and strong tropical land carbon uptake from vertical profiles of atmospheric CO_2, Science, 316, 1732–1735, 2007. 28171
Stull, R. B.: An Introduction to Boundary Layer Meteorology, Kluwer Academic Publishers, 1988. 28172, 28173, 28177, 28179, 28182
Sun, W. and Ogura, Y.: Modeling the evolution of the concevtice Planetary Boundary-Layer, J. Atmos. Sci., 37, 1558–1572, 1980. 28184
Tolk, L. F., Meesters, A. G. C. A., Dolman, A. J., and Peters, W.: Modelling representation errors of atmospheric CO_2 mixing ratios at a regional scale, Atmos. Chem. Phys., 8, 6587–6596, doi:10.5194/acp-8-6587-2008, 2008. 28171
Tolk, L. F., Peters, W., Meesters, A. G. C. A., Groenendijk, M., Vermeulen, A. T., Steeneveld, G. J., and Dolman, A. J.: Modelling regional scale surface fluxes, meteorology and CO_2 mixing ratios for the Cabauw tower in the Netherlands, Biogeosciences, 6, 2265–2280, doi:10.5194/bg-6-2265-2009, 2009. 28171
van der Molen, M. K. and Dolman, A. J.: Regional carbon fluxes and the effect of topography on the variability of atmospheric CO_2, J. Geophys. Res.-Atmos., 112, D01104, doi:10.1029/2006JD007649, 2007. 28171
Vogelezang, D. and Holtslag, A.: Evaluation and model impacts of alternative boundary-layer height formulations, Bound.-Lay. Meteorol., 81, 245–269, 1996. 28181
Wofsy, S., Harris, R., and Kaplan, W.: Carbon-Dioxide in the atmosphere over the amazon basin, J. Geophys. Res.-Atmos., 93, 1377–1387, 1988. 28172, 28178
Yi, C., Davis, K., Berger, B., and Bakwin, P.: Long-term observations of the dynamics of

ACPD
11, 28169–28217, 2011

the continental planetary boundary layer, J. Atmos. Sci., 58, 1288–1299, doi:10.1175/1520-0469(2001)058¡1288:LTOOTD¿2.0.CO;2, 2001a. 28179

Yi, C. X., Davis, K. J., Berger, B. W., and Bakwin, P. S.: Long-term observations of the dynamics of the continental planetary boundary layer, J. Atmos. Sci., 58, 1288–1299, 2001b. 28171, 28172

Yi, C., Davis, K. J., Bakwin, P. S., Denning, A. S., Zhang, N., Desai, A., Lin, J. C., and Gerbig, C.: Observed covariance between ecosystem carbon exchange and atmospheric boundary layer dynamics at a site in northern Wisconsin, J. Geophys. Res.-Atmos., 109, D08302, doi:10.1029/2003JD004164, 2004. 28171, 28173

ACPD

11, 28169–28217, 2011

Table 1. Setup of WRF options.

Option	Setting
Model code version	3.0.1.1
Time step integration	1 min, 3rd order Runge-Kutta, output intervall 1 h
Grid definition	280 × 400 (North-South × West-East), 10 km spacing, Arakawa C
Vertical coordinates	41 levels (20 below 2 km), terrain following, eta coordinates, pressure top 50 hPa
Basic equations	Non-hydrostatic, compressible
Microphysics	WRF single moment class 5
Atmospheric radiation	Rapid Radiative Transfer Model (RRTM, long wave), Mesoscale Model 5 (MM5, Dudhia, short wave)
Cumulus parameterization	Kain-Fritsch scheme, calculated every 5th time step
Land-Surface Model (LSM)	Noah LSM, 4 soil layers
PBL scheme	Yonsei University (YSU setting), Mellor-Yamada-Janjic (MYJ setting)
Surface layer scheme	Monin-Obukhov similarity (YSU setting), Monin-Obukhov (Janjic Eta, MYJ setting)

ACPD
11, 28169–28217, 2011

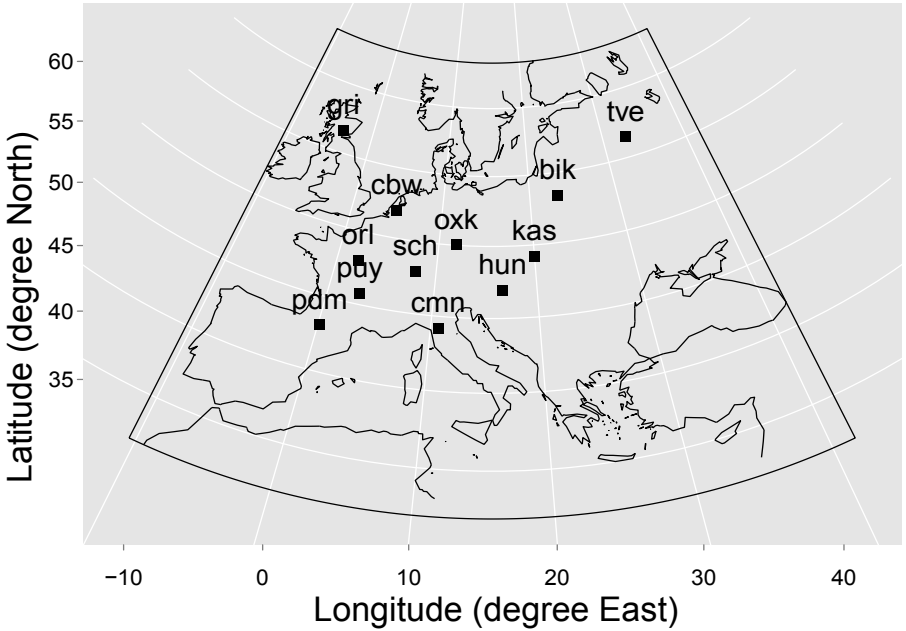

Fig. 1. Spatial domain of the WRF-VPRM simulations. Squares indicate the location of continuous CO_2 measurement sites. The model grid cells containing these stations were used for point comparisons.

ACPD
11, 28169–28217, 2011

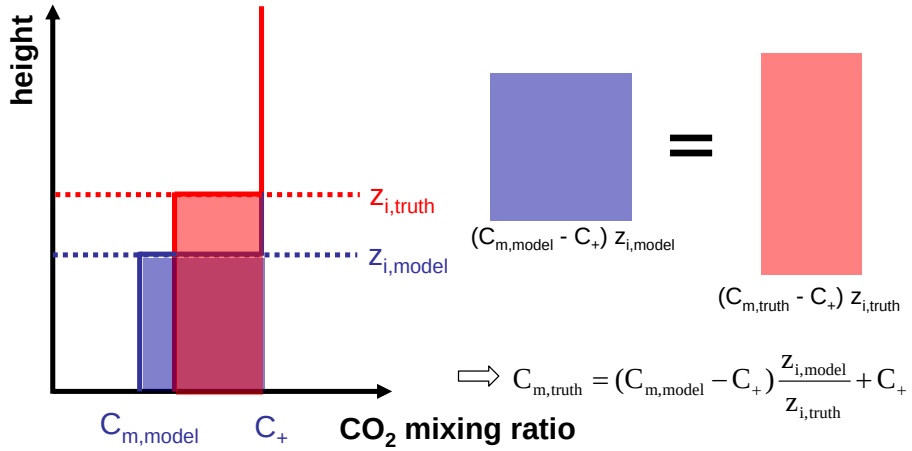

Fig. 2. Idealized CO_2 profiles in a column of air with unit area. A model with weak vertical mixing (blue lines) has a lower mixing height ($z_{i,model}$) than the truth ($z_{i,truth}$, red lines). The shaded areas represent the mixed layer column mass assuming a constant air density profile. The reshuffling method (Eq. 2) scales the modeled ML CO_2 such the column mass keeps unchanged.

ACPD
11, 28169–28217, 2011

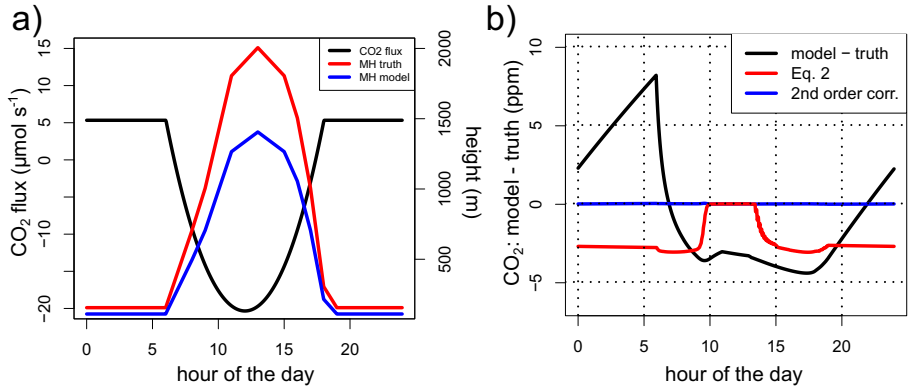

Fig. 3. The surface fluxes (F_{NEE}) used for the 1-D conceptual model (Eq. 3) with 24 h mean ~3.4 µmoles s^{-1}, also shown are the prescribed mixing heights for the truth (red line) and the model with a 30 % low bias (blue line) **(a)**. Also shown in **(b)** is the Diurnal variation of the CO_2 difference ($C_{m,model} - C_{m,truth}$) (black line) resulting from 1-D conceptual model (Eq. 3). The red line shows the same error after applying the reshuffling method (Eq. 2) to the model ML CO_2 ($C_{m,model}$). Taking into account the residual layer mole fraction completely compensates for the difference (blue line).

ACPD
11, 28169–28217, 2011

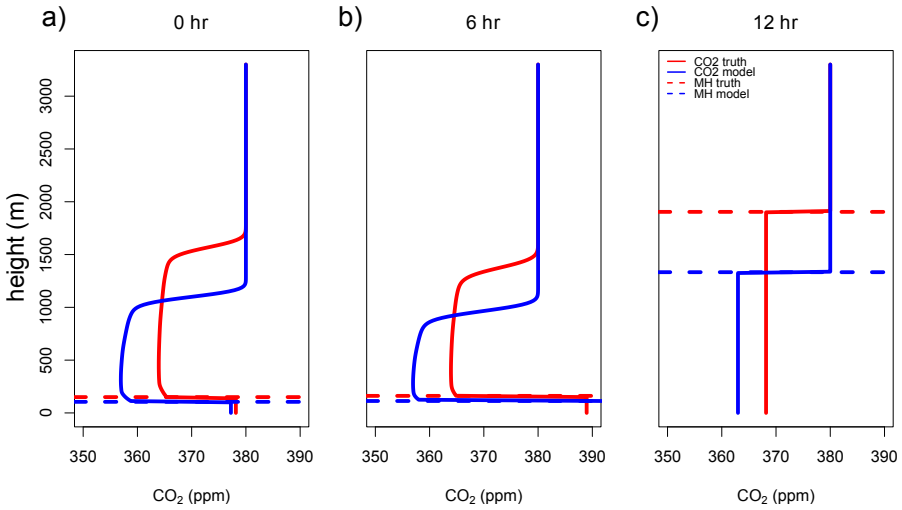

Fig. 4. Three profiles calculated by the conceptual model (Eq. 3) for the model (blue line) and the truth (red line) at different times of the day (vertical lines): during night time **(a)** and in the morning **(b)** a residual layer remains from the previous day above the ML (dashed horizontal lines). At noon the residual layer was completely entrained **(c)**.

ACPD
11, 28169–28217, 2011

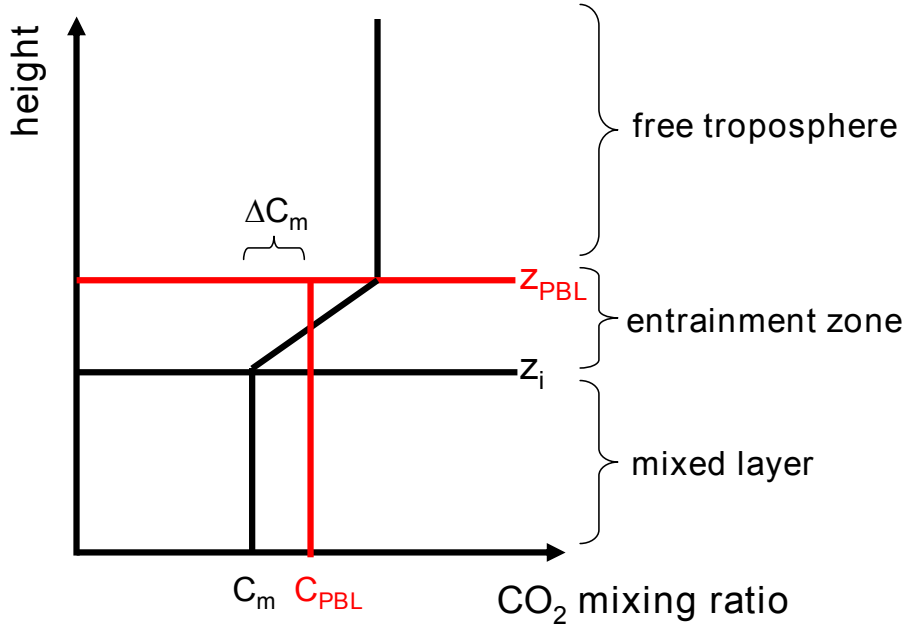

Fig. 5. Illustration of the effect of differences between the mixing height (z_i) and a diagnosed PBL top (z_{PBL}) on the ML mean mole fraction (C_m). The column mixing ratio integrated from the surface to z_{PBL} has a higher value than a similar column integrated to the top of the well mixed part (z_i). The difference between these two mean mixing ratios is shown as ΔC_m.

ACPD
11, 28169–28217, 2011

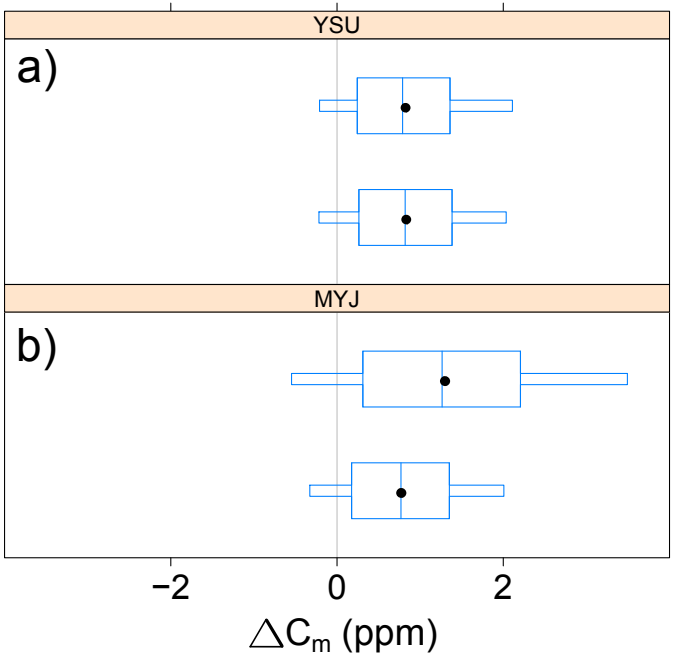

Fig. 6. Box and whisker plot of ΔC_m for monthly averaged mean ML CO_2 for YSU **(a)** and MYJ **(b)** at 12:00 UTC. All grid cells were included in the boxplot where the diagnosed PBL top was higher than 600 m in both simulations. The upper boxes represent the differences of mean CO_2 integrated over the offline diagnosed MH (VH96 Eq. 1, $Ri_c = 0.25$) and the mean CO_2 integrated over 300 m (within the well mixed part of the ML). The lower boxes show similar differences but using online diagnosed WRF PBL top and the 300 m height. The whiskers denote the central 90 % of the data points, the boxes the central 50 %, the vertical lines within the boxes are the median and the black dots represent the mean.

ACPD
11, 28169–28217, 2011

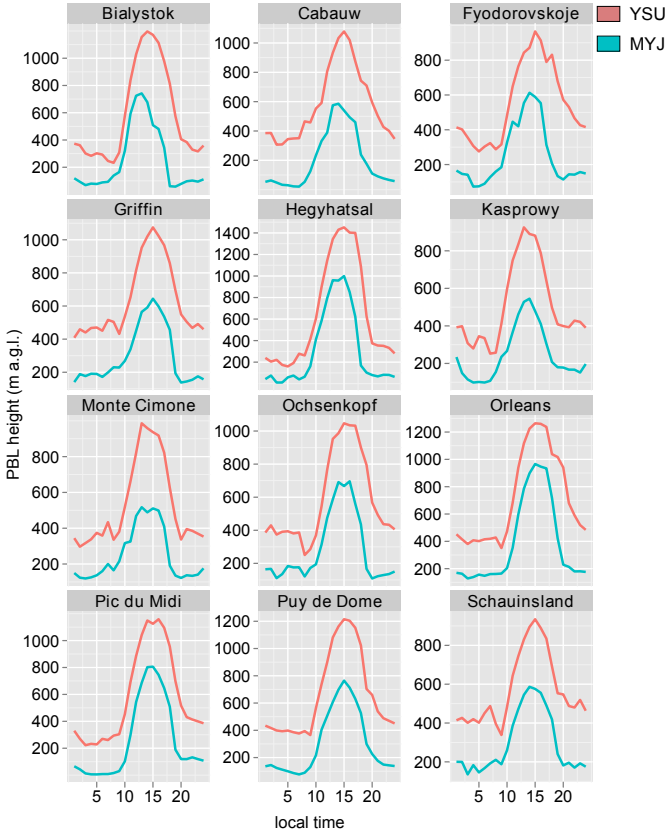

Fig. 7. Mean diurnal MH in m (a.g.l.) at grid cells containing the stations (from top to bottom, left to right): BIK, CBW, TVE, GRI, HUN, KAS, CMN, OXK, ORL, PDM, PUY and SCH. Results from the YSU and MYJ simulations are shown in red lines and cyan lines respectively.

ACPD
11, 28169–28217, 2011

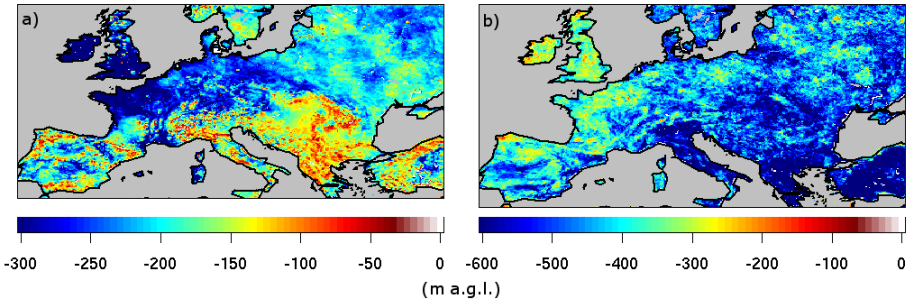

Fig. 8. Time averaged MH differences for all land grid cells $< z_{i,\mathrm{myj}} - z_{i,\mathrm{ysu}} >$ in meter above ground level at 01:00 UTC **(a)** and 12:00 UTC **(b)**.

ACPD
11, 28169–28217, 2011

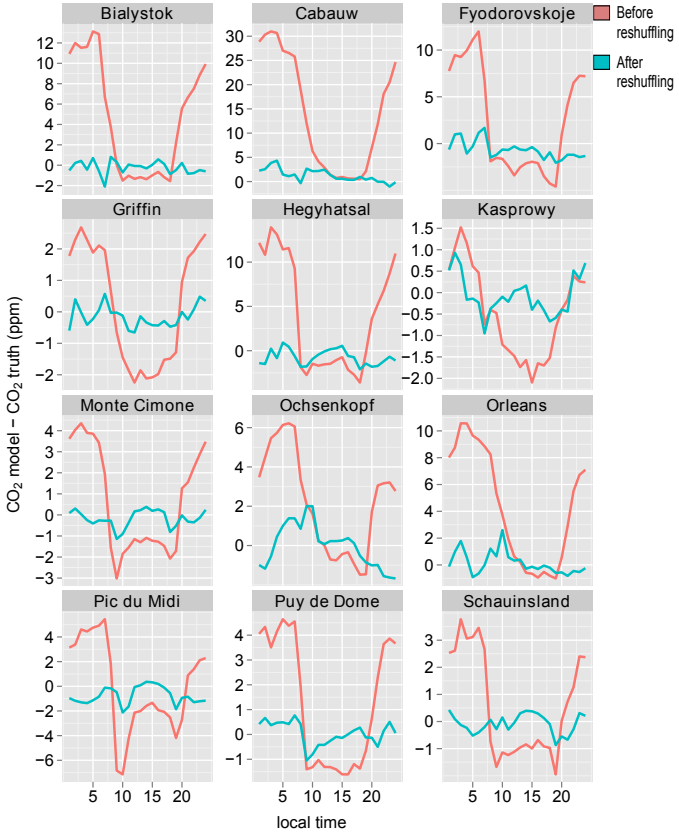

Fig. 9. Same as Fig. 7 but for the bias in ML CO_2 ($< C_{m,myj} - C_{m,ysu} >$, red line) and the bias after applying the reshuffling method (Eq. 2) to the MYJ CO_2 fields (cyan line).

ACPD
11, 28169–28217, 2011

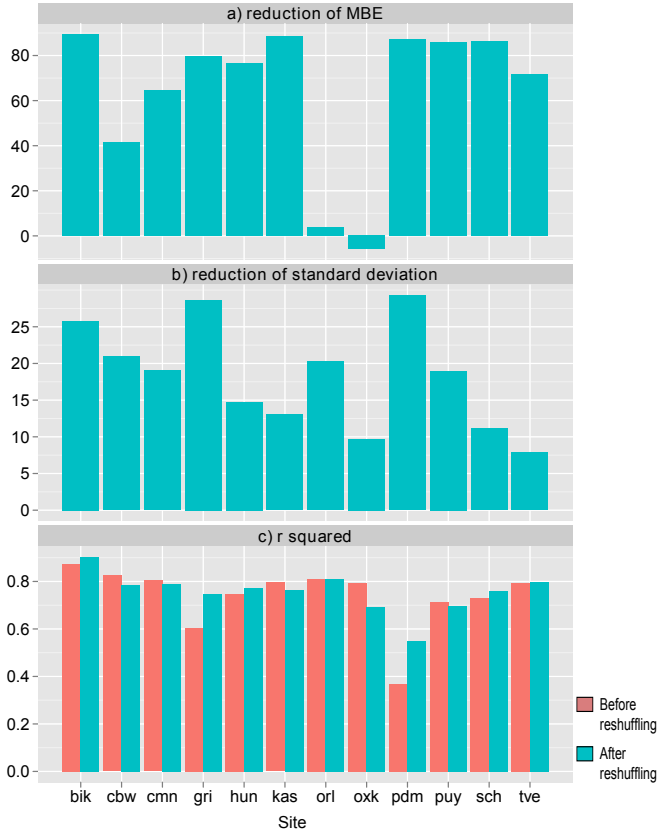

Fig. 10. Summary barplot of the error reduction (in %) **(a)**, reduction of random error (in %) **(b)** and correlation before (red) and after the reshuffling was applied (cyan) **(c)**. The results show averages for daytime (10:00–18:00 local time).

ACPD
11, 28169–28217, 2011

Error characterization of CO_2 vertical mixing

R. Kretschmer et al.

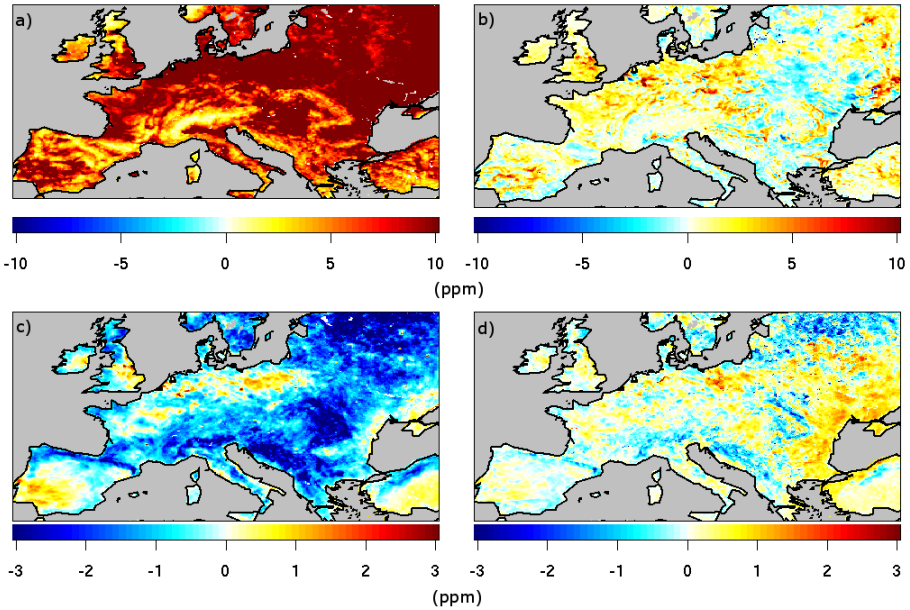

Fig. 11. Monthly mean ML CO_2 difference ($C_{m,myj} - C_{m,ysu}$) for each land grid cell at 01:00 **(a)** and 12:00 UTC **(c)**. The bias after applying the offline reshuffling method (Eq. 2) to the MYJ mixing ratios is shown for 01:00 **(b)** and 12:00 UTC **(d)**.

ACPD
11, 28169–28217, 2011

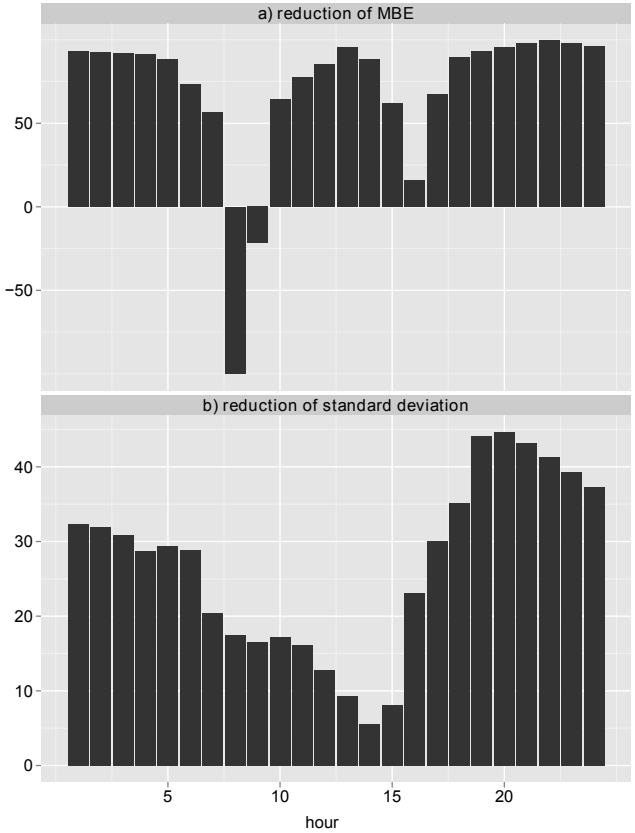

Fig. 12. Summary barplot of the bias reduction **(a)** and reduction of random error **(b)** in per cent. One bar represents the average over all land grid cells in the domain at one hour of the day.

ACPD
11, 28169–28217, 2011

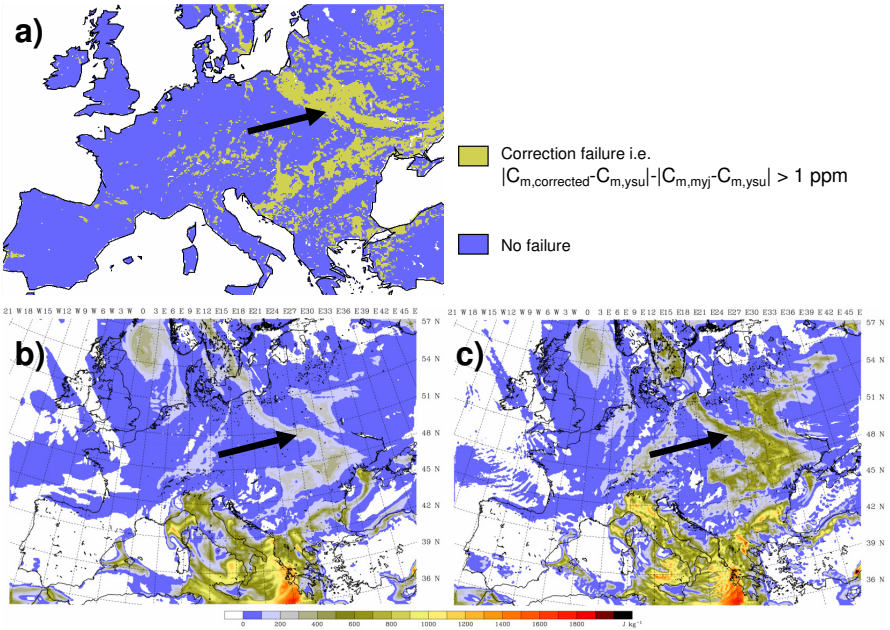

Fig. 13. Grid cells for which the reshuffling method failed calculated for 10 August 2006, 12:00 UTC **(a)**. Also shown is the Convective Available Potential Energy (CAPE) for YSU **(b)** and MYJ **(c)** at the same time. Details are given in the text.

ACPD
11, 28169–28217, 2011